of course, would be expected for the exculsive complexes where the solvent has an ample opportunity to interact with the unshielded side of the cation.

Acknowledgment. The authors gratefully acknowledge the support of this work by the National Science Foundation, Grant No. CHE-077-12541.

Registry No. C222·K$^+$, 32611-95-3; C221·K$^+$, 32611-87-3; C211·K$^+$, 32824-90-1; K$^+$, 24203-36-9.

Contribution from University Chemical Laboratories, Cambridge CB2 1EW, England

Spectra and Magnetism of Triclinic Crystals of Tetra-*n*-butylammonium Tribromo(quinoline)cobaltate and -nickelate

MALCOLM GERLOCH* and LYALL R. HANTON

Received October 29, 1979

The magnitudes and orientations of the principal paramagnetic susceptiblities of triclinic crystals incorporating the complex ions M(quinoline)Br_3^- (M = Ni(II), Co(II)) have been measured throughout the temperature range 20–300 K. Unpolarized crystal transmission spectra have been recorded in the range 4000–26 000 cm^{-1} at 4 K, that for the cobalt complex confirming and augmenting previously published data. Quantitative agreement with all these data and also with the single-crystal ESR **g** tensor, reported by Bencini and Gatteschi for the cobalt complex, has been achieved with the angular-overlap model. Values for all AOM, interelectron repulsion, and spin–orbit coupling parameters have been defined. The quinoline ligand has been shown to act as a π acceptor in both complexes. The spin–orbit coupling coefficient appears anomalously small in the nickel complex.

Introduction

Current techniques for magnetochemistry and ligand field theory provide means to determine, in a semiquantitative manner, the separate extents of σ and π bonding between the metal and each ligand within a transition-metal complex.[1] In what may be regarded still as a developmental phase in the exploitation of the angular overlap model as applied to paramagnetic susceptibilities, ESR *g* values, and the d–d electronic spectra, our concern in any given study must be as much with establishing norms as with characterizing new bonding features and, at the same time, with testing the capacity of the method in ever more exacting circumstances.

The subject of the present study is the isomorphous pair of complex ions M(Q)Br_3^-, where M = Ni(II) and Co(II) and Q = quinoline. Of immediate chemical interest are the π-bonding roles of bromine and quinoline in these nominally tetrahedral species and a comparison of the π-bonding function of quinoline here with that of pyridine in other complexes which have been analyzed[2] in a similar way. A particular challenge, so far as both practical and theoretical techniques are concerned, centers on the triclinic nature of the lattice in which these complex ions crystallize[3] with tetra-*n*-butylammonium cations. We report here complete determinations of the triclinic crystal susceptibilities of each complex throughout the temperature range 20–300 K, using methods recently developed[4] for the measurement of the antiferromagnetism of several binuclear cobalt benzoates.[4,5] The present experiments describe the first successful measurements of triclinic paramagnets since the early work on $CuSO_4 \cdot 5H_2O$: a recent study[7] of the paramagnetism of a triclinic crystal did not experimentally establish both magnitudes and orientations of the principal susceptibilities as is done here. Set against the considerable difficulty in measuring triclinic susceptibilities are two advantages. Except where there are two or more paramagnetic centers in the crystallographic asymmetric unit, and this is not the case here, there is equality by identity between the crystal and molecular susceptibilities under circumstances of effective magnetic dilution. Further, the increased data set provided by the determination of the magnitudes and all orientations of the principal susceptibilities provides a more exacting property for the theoretical model to reproduce. The situation is particularly attractive in the present study in view of the relatively small number of parameters required to describe σ and π bonding from only two ligand types, one of which (bromine) is considered to π bond symmetrically about the metal–ligand axis and the other of which probably π bonds in one direction only (though this is to be verified).

We also report single-crystal, unpolarized, transmission spectra for both complexes down to liquid-helium temperatures, those for the cobalt complex confirming the detailed, polarized spectra reported elsewhere.[8] The magnitudes and orientations of the principal molecular *g* values of the cobalt complex have also been reported recently.[9] We have established parameter values which simultaneously reproduce all details of susceptibility, optical spectra, and, as appropriate, ESR properties in these two complexes, demonstrating a significant π-acceptor role for the quinoline ligands. The study also contributes to evidence of anomalous spin–orbit coupling in tetrahedral nickel(II) complexes.

Experimental Section

The complex salts $[(n\text{-}C_4H_9)_4N][M(C_9H_7N)Br_3]$ (M = Co, Ni) were prepared by the published method,[3] and satisfactory CNH analyses were obtained. Large crystals were prepared by slow evaporation of the reaction mixtures and also by recrystallization from butanol.

Susceptibilities. All susceptibility measurements were performed on crystals weighing 1–4 mg, by using our single-crystal Faraday balance[10] and procedures recently described.[4] As the present work is the first complete susceptibility study of a triclinic *paramagnet* for many years and the first based solely upon the Faraday method, we briefly review the procedure followed. The first stage follows that of Ghosh and Bagchi,[11] involving the measurement of the average

(1) M. Gerloch, *Prog. Inorg. Chem.*, **26**, 1 (1979).
(2) M. Gerloch, R. F. McMeeking, and A. M. White, *J. Chem. Soc., Dalton Trans.*, 2452 (1975).
(3) W. D. Horrocks, Jr., D. H. Templeton, and A. Zalkin, *Inorg. Chem.*, **7**, 2303 (1968).
(4) P. D. W. Boyd, J. E. Davies, and M. Gerloch, *Proc. R. Soc. London, Ser. A*, **360**, 191 (1978).
(5) J. E. Davies and M. Gerloch, in preparation.
(6) K. S. Krishnan and A. Mookerji, *Phys. Rev.*, **50**, 860 (1936); **54**, 533, 841 (1938).
(7) S. Mitra, B. N. Figgis, C. L. Raston, B. W. Skelton, and A. H. White, *J. Chem. Soc., Dalton Trans.*, 753 (1979).
(8) I. Bertini, D. Gatteschi, and F. Mori, *Inorg. Chim. Acta*, **7**, 717 (1973).
(9) A. Bencini and D. Gatteschi, *Inorg. Chem.*, **16**, 2141 (1977).
(10) D. A. Cruse and M. Gerloch, *J. Chem. Soc., Dalton Trans.*, 152 (1977).

0020-1669/80/1319-1692$01.00/0

Table I. Tetra-*n*-butylammonium Tribromo(quinoline)nickelate: Experimental Values of Maximum and Minimum Susceptibilities in Planes Perpendicular to the Zone Axes [*u*, *v*, *w*], in 10^4 cgsu[a]

T, K	[111]	[001]	[110]	[100]	[101]	[112]	[11$\bar{1}$]	[010]
295	62	53	57	60	60	64	50	50
	42	43	47	44	42	42	47	44
275	70	60	62	65	66	68	54	53
	44	46	49	47	45	44	50	46
255	78	66	68	75	73	75	58	57
	47	50	53	52	48	48	53	49
235	84	72	73	82	80	82	62	62
	50	54	57	56	51	51	57	53
215	92	79	30	90	87	90	68	67
	54	57	62	61	55	54	62	57
195	102	86	88	100	96	99	74	74
	59	61	67	67	60	59	67	62
175	114	95	97	111	107	110	82	82
	65	67	74	74	65	64	74	68
155	128	106	109	126	121	124	92	92
	72	73	82	83	72	70	82	76
135	149	122	124	145	138	143	104	105
	80	81	93	94	80	78	92	85
115	176	142	145	172	163	168	122	120
	92	92	106	109	91	88	106	96
95	215	170	176	211	200	205	146	144
	108	105	125	130	106	102	125	111
75	283	216	223	277	261	268	184	180
	129	124	154	162	127	122	153	134
55	398	295	300	391	362	375	245	238
	157	149	196	211	156	150	194	165
35	646	447	464	637	573	601	358	342
	186	181	262	294	194	187	258	202
25	909	563	624	899	791	839	470	433
	187	195	309	360	211	201	304	223

[a] 1 cgsu = $4\pi \times 10^{-6}$ m^3 mol^{-1}.

Table II. Tetra-*n*-butylammonium Tribromo(quinoline)cobaltate: Experimental Values of Maximum and Minimum Susceptibilities in Planes Perpendicular to the Zone Axes [*u*, *v*, *w*], in 10^4 cgsu[a]

T, K	[001]	[100]	[010]	[10$\bar{1}$]	[01$\bar{1}$]	[10$\bar{2}$]	[101]	[111]
295	96	87	94	94	92	90	93	95
	87	81	85	87	85	83	84	81
275	103	95	101	99	99	96	99	102
	92	86	91	93	91	89	90	86
255	110	101	109	107	106	103	107	109
	99	92	97	100	97	95	96	92
235	119	109	118	116	114	111	116	119
	107	99	105	108	105	103	104	99
215	131	120	128	126	125	122	126	130
	116	107	114	116	114	112	112	108
195	144	131	141	138	139	134	139	143
	128	117	125	127	126	123	124	118
175	160	145	157	153	155	149	154	159
	142	129	139	141	139	136	137	130
155	181	162	177	171	174	169	174	179
	158	144	155	157	156	153	152	144
135	208	185	204	196	201	194	199	205
	180	163	176	177	179	174	173	163
115	245	216	240	229	238	228	234	242
	209	188	205	206	209	203	200	187
95	300	260	294	277	292	278	284	294
	250	222	245	245	252	243	238	220
75	389	331	381	355	381	357	367	380
	315	274	309	305	319	307	296	271
55	545	446	531	483	534	490	509	531
	415	351	409	399	426	404	386	346
35	904	674	872	755	881	787	826	876
	623	478	603	575	637	587	550	471
25	1322	904	1278	1037	1287	1118	1182	1267
	804	575	794	737	845	767	699	565

[a] 1 cgsu = $4\pi \times 10^{-6}$ m^3 mol^{-1}.

susceptibility in a plane perpendicular to a chosen crystal axis having direction cosines $\xi\eta\zeta$ with respect to a fixed crystal reference frame (here a, c^*, $a \times c^*$):

$$2\bar{\chi}_{\xi\eta\zeta} = \chi_{max} + \chi_{min} = \chi_{11}(1 - \xi^2) + \chi_{22}(1 - \eta^2) + \chi_{33}(1 - \zeta^2) - 2(\chi_{12}\xi\eta + \chi_{13}\xi\zeta + \chi_{23}\eta\zeta) \quad (1)$$

Such values of $\bar{\chi}$ were measured for several crystal orientations, the latter being established by conventional X-ray oscillation and Weissenberg photography and with computational aids[12] devised by Dr. J. E. Davies. The method requires knowledge only of the crystal mass and of the force upon it in the magnetic field and that the crystal be oriented within ca. 1.5° of the chosen axis, parallel to the mounting fiber. There is no measurement of, or requirement for, the orientation of χ_{max} with respect to the magnetic field vector. In principle, measurements perpendicular to six axes yield simultaneous equations from which all six independent elements of the crystal susceptibility tensor may be deduced: a similar process is followed at each of several temperatures chosen throughout the experimental range 20–300 K. In practice, however, the linear independence of the equations may be insufficiently established, either by unfortunate choices of some of the experimental crystal orientations or because of experimental errors being significant in comparison with the differences between $\bar{\chi}$ values from different axes. As will be described, we have measured susceptibilities perpendicular to eight different suspension axes.

The second stage, developed recently,[4] utilizes the individual values of χ_{max} and χ_{min} of (1) rather than just their sum. Using the total χ tensor from the first stage as the point of departure, a least-squares process provides a more accurate tensor by refinement of the $2n$ pieces of data measured for n crystal mountings. The correct equations used here (replacing those misprinted but correctly used in ref 4) are

$$\chi_{max} = a_{11}^2\chi_{11} + a_{12}^2\chi_{22} + a_{13}^2\chi_{33} + 2a_{11}a_{12}\chi_{12} + 2a_{11}a_{13}\chi_{13} + 2a_{12}a_{13}\chi_{23} \quad (2a)$$

$$\chi_{min} = a_{21}^2\chi_{11} + a_{22}^2\chi_{22} + a_{23}^2\chi_{33} + 2a_{21}a_{22}\chi_{12} + 2a_{21}a_{23}\chi_{13} + 2a_{22}a_{23}\chi_{23} \quad (2b)$$

where χ_{max} is taken as the greater of these two expressions and the a_{ij} express the orientation of χ_{max} and χ_{min} in each experimental plane, established by the preceding least-squares cycle or initially from the first stage of Ghosh and Bagchi.

In Tables I and II are listed interpolated observed values of χ_{max} and χ_{min} throughout the experimental temperature range for $[(n\text{-}C_4H_9)_4N][M(C_9H_7N)Br_3]$ (M = Ni, Co), all values being corrected for an average diamagnetism of $\chi_M^{dia} = 398 \times 10^{-6}$ cgsu calculated from Pascal's constants.[13] Derived values of the principal crystal susceptibilities and moments and their orientations, obtained from eq 2 and the procedures of ref 4, are given in Table III.

The processes of measuring the susceptibilities of triclinic crystals used here are new, and general, and it is important to demonstrate their reliability and self-consistency, as follows:

(i) We have measured χ_{max} and χ_{min} for each axis of suspension, giving 16 pieces of data from which are determined the six independent tensor elements by least squares. Back-calculation from these refined tensor elements yields values of χ_{max} and χ_{min} which may be compared with the input observed data. Expressing agreement by an index $R = \sum_{temp}|\chi_{obsd} - \chi_{calcd}|/\chi_{obsd}$ for χ_{max} and χ_{min} for each axis, we find R factors ranging from 0.012 to 0.055 for the nickel complex, with an average R value of 0.020, and for the cobalt system R ranging from 0.007 to 0.032 with an average of 0.017.

(ii) For the nickel complex, with $\bar{\chi}$ values from six suspension axes, the first stage failed to produce a sufficiently accurate tensor from which the least-squares second stage could refine. This was due to a combination of inevitable experimental errors and to an unfortunate choice of suspension axes in that four of the six directions all lay in a plane. Even with data from seven axes, the least-squares process failed to converge with data at some temperatures. The results in Table I were obtained from all the data collected from the eight axes shown. However, it is interesting to compare results from the complete "self-solving" data from eight axes with those obtained from only five axes taken together with the assumption that one principal susceptibility lies parallel to the Ni–N(Q) vector. The assumption was only used for the first stage to provide a starting point for the least-squares

(11) U. S. Ghosh and R. N. Bagchi, *Indian J. Phys.*, **36**, 538 (1962).
(12) J. E. Davies, personal communication.
(13) F. G. Mabbs and D. J. Machin, "Magnetism and Transition Metal Complexes", Chapman and Hall, London, 1973, p 5.

Table III. Principal Susceptibilities and Moments and Their Orientations with Respect to the Orthogonalized Crystal Axes (a, c^*, $a \times c^*$)

	Ni complex					Co complex				
			Ni complex orientation, deg					Co complex orientation, deg		
T, K	$10^{-4}\chi$, cgsu	μ, μ_B				$10^{-4}\chi$, cgsu	μ, μ_B			
295	62	3.84	93.4	27.1	116.9	96	4.76	34.3	55.8	92.4
	47	3.33	68.2	63.9	35.1	85	4.49	115.5	47.5	53.2
	42	3.15	22.1	96.9	110.9	83	4.43	68.6	118.5	36.9
275	69	3.89	92.1	24.7	114.6	103	4.76	42.8	47.7	95.2
	50	3.31	69.8	66.3	32.0	90	4.45	132.3	45.2	103.0
	44	3.12	20.4	96.5	109.2	90	4.44	95.0	76.9	14.1
255	77	3.97	90.6	25.6	115.5	111	4.75	37.8	52.6	94.7
	54	3.31	70.8	65.8	31.7	97	4.44	123.5	40.2	70.4
	47	3.11	19.2	97.7	107.5	96	4.42	74.6	102.7	20.2
235	84	3.98	90.4	25.1	115.1	120	4.75	39.0	51.4	94.9
	58	3.30	71.1	66.3	31.1	104	4.42	126.6	39.4	77.6
	51	3.09	18.9	97.5	107.2	104	4.41	78.4	96.7	13.4
215	92	3.98	90.4	24.9	114.9	131	4.75	40.2	50.3	95.0
	63	3.29	72.8	66.2	30.0	113	4.41	127.5	40.6	76.6
	54	3.06	17.2	96.8	105.7	112	4.39	77.6	97.2	14.4
195	102	3.99	90.1	25.7	115.7	144	4.75	28.4	61.7	92.4
	69	3.27	74.9	65.3	29.5	127	4.45	110.5	45.2	51.9
	59	3.03	15.1	96.4	103.6	120	4.33	71.2	121.9	38.2
175	114	3.99	89.9	25.9	115.9	160	4.73	7.4	96.4	93.7
	76	3.25	75.7	65.0	29.3	144	4.49	96.8	125.6	143.6
	64	3.00	14.3	96.2	102.8	130	4.27	87.0	36.3	126.1
155	128	3.99	89.7	25.9	115.9	181	4.73	6.7	95.8	93.4
	84	3.23	76.2	64.9	29.1	161	4.47	96.1	123.0	146.3
	71	2.96	13.8	96.2	102.3	145	4.24	87.1	33.6	123.5
135	148	4.00	89.7	26.0	116.0	207	4.73	8.3	98.1	91.7
	95	3.21	77.1	64.8	28.7	185	4.47	96.2	125.7	143.6
	79	2.91	12.9	95.8	101.5	163	4.20	84.5	36.9	126.4
115	175	4.01	90.0	25.8	115.8	245	4.74	7.9	97.6	92.2
	109	3.17	78.4	64.7	28.2	216	4.45	96.3	125.8	143.4
	89	2.86	11.6	95.1	100.4	188	4.16	85.2	36.9	126.5
95	214	4.03	89.8	26.0	116.0	300	4.77	7.1	97.0	91.6
	130	3.14	79.6	64.5	27.9	260	4.44	95.4	126.3	143.1
	103	2.79	10.4	94.7	99.3	222	4.11	85.4	37.2	126.8
75	281	4.10	89.3	26.1	116.1	389	4.83	6.4	96.2	91.7
	160	3.10	80.6	64.4	27.5	330	4.45	95.0	125.8	143.7
	122	2.71	9.4	94.8	98.1	273	4.05	86.0	36.5	126.2
55	395	4.17	89.0	25.7	115.7	547	4.90	6.8	95.9	93.2
	206	3.01	81.6	64.7	26.8	444	4.42	96.1	125.1	144.2
	147	2.54	8.4	94.5	97.1	350	3.92	87.1	35.8	125.6
35	641	4.24	89.3	26.3	116.3	909	5.05	6.9	95.7	93.8
	279	2.79	81.9	64.1	27.3	673	4.34	96.4	124.9	144.4
	175	2.22	8.1	94.2	96.9	476	3.65	87.5	35.5	125.3
25	901	4.24	89.4	27.3	117.3	1335	5.17	6.2	94.7	94.0
	328	2.56	81.5	63.1	28.4	900	4.24	96.0	124.4	144.9
	185	1.92	8.5	94.5	97.2	576	3.39	88.4	34.8	124.8

Table IV. Progress of χ Measurements for the Nickel Complex

	data from first 5 axes				data from all 8 axes			
T, K	$10^{-4}\chi$, cgsu	orientation, deg			$10^{-4}\chi$, cgsu	orientation, deg		
295	62	79.4	79.3	15.2	62	81.0	81.0	12.8
	47	69.6	158.5	83.5	47	75.1	163.7	83.5
	42	23.2	71.6	103.7	42	17.5	76.5	101.0
25	915	68.9	76.0	25.7	901	77.0	81.2	15.8
	360	83.1	165.9	77.7	328	89.0	171.2	81.2
	184	22.3	88.2	112.2	185	13.1	91.0	103.0

Table V. Comparison of Constrained and Unconstrained χ Tensors for the Nickel Complex

T, K	$10^{-4}\chi$,[a] cgsu	$10^{-4}\chi$,[b] cgsu
295	54	62
	53	47
	43	42
25	992	901
	323	328
	86	185

[a] Using the first five axes with maximum χ constrained to lie parallel to Ni-N. [b] Using all eight axes without constraints.

refinement: we observe close agreement with the tensor from the complete data after this process is completed, as shown in Table IV.

From the first tensor (Table I), we note that the largest susceptibility lies 13° from Ni–N at 295 K and 16° at 25 K (i.e., probably equal within experimental error), so that even a rough initial assumption can help to begin the refinement process. This is not to say that such an assumption is adequate for the calculation of the magnitudes of the principal susceptibilities, however. Comparing data from the same five axes and the total set of eight once more, but now maintaining the fiction that one principal susceptibility lies exactly parallel to the Ni–N vector, gives the results shown in Table V. We must conclude from these that it is generally unacceptable to presume knowledge of the directions of any principal molecular susceptibilities in the absence of any rigorous defining symmetry elements.

(iii) For the cobalt complex, the overall anisotropy of the cobalt analogue is less than for the nickel one, as expected for a ground term devoid of orbital angular momentum. We anticipated, therefore, that this system would provide a particularly severe test of the experimental procedures for the determination of triclinic susceptibilities. Despite this, the progress of measurement of the cobalt susceptibilities followed a similar course to that for the nickel one. We note that the orientation of the susceptibility tensor here is significantly different from that for the nickel one (Table III and Figure 1), again demonstrating that directions of principal molecular susceptibilities should not be assumed solely on the basis of *approximate* molecular symmetry. The same point was made by Bencini and Gatteschi in their ESR study[9] of this complex. In Table VI we list their principal g values and orientations relative to the same frame used in Table III. Note that the orientations of the g values and χ tensors are closely similar.

Spectra. Crystal transmission spectra were recorded in the range 4000–26 000 cm^{-1} by using a Cary 14R spectrophotometer. Suffi-

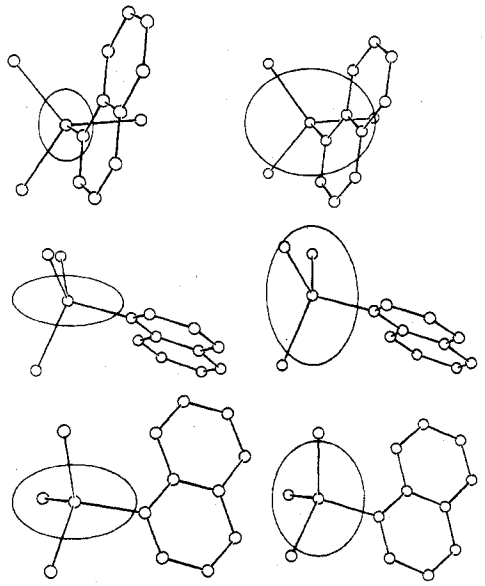

Figure 1. Projections of the susceptibility magnitude ellipsoids down directions of the principal susceptibilities at 25 K, shown for the nickel complex on the left and for the cobalt complex on the right. Relative scale for nickel:cobalt is approximately 1:5 with respect to values listed in Table III. Ellipses for observed and calculated susceptibilities coincide within the scale of the drawings throughout the temperature range 20–300 K.

Table VI. Tetra-*n*-butylammonium Tribromo(quinoline)cobaltate: Observed Principal *g* Values and Their Orientations with Respect to the Orthogonalized Frame Used for Table III (Transformed from the Data in Ref 9) Compared with Those Calculated with the Parameter Set in Table X

obsd				calcd			
g	orientation, deg			*g*	orientation, deg		
6.51	0.8	89.4	90.6	6.52	11.3	100.8	93.2
2.33	90.1	127.5	142.5	2.36	96.6	109.8	159.0
1.61	90.9	37.5	127.5	1.66	81.0	22.6	110.7

ciently transparent crystals of these darkly colored materials could only be ground for experiments with light incident on the (010) face. Spectra were recorded at room temperature and at those of liquid nitrogen and liquid helium. Some degree of band sharpening was observed on cooling of the crystal, the best resolved bands occurring on spectra at ca. 4 K and shown in Figures 2 and 3. Also shown in Figure 2 are markers for the peak maxima obtained by Bertini et al.[8] from their polarized spectral data. Our results are in good agreement with this more resolved study, but we draw attention to the weak, broad feature around 12 000 cm^{-1}.

Discussion

Our theoretical approach,[14] exploiting the angular overlap model (AOM), has been used recently in the study of ligand field properties of various transition-metal complexes. Calculations have been performed within bases spanning the complete spin-triplet manifold—$^3F + {}^3P$—and later the complete d^8 configuration for the nickel complex and the complete spin-quartet manifold—$^4F + {}^4P$—and subsequently the complete d^7 configuration for the cobalt complex. Ligand coordinates and orientations were taken as defined by the X-ray structural analysis.[3] The models are parameterized by B or F_2 and F_4 (depending on basis size) for interelectron repulsion, by ζ and k for spin–orbit coupling and Stevens' orbital reduction effect, and by the ligand field AOM parameters e_σ(Br) and e_σ(Q) for σ interaction of the metal with bromine and

(14) M. Gerloch and R. F. McMeeking, *J. Chem. Soc., Dalton Trans.*, 2443 (1975).

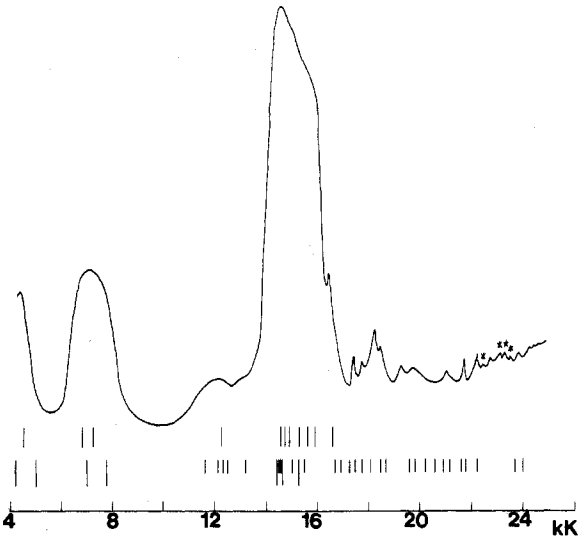

Figure 2. Tetra-*n*-butylammonium tribromo(quinoline)cobaltate unpolarized crystal transmission spectrum at ca. 4 K. Bars indicate calculated eigenvalues: long for quartets, short for doublets. Also shown are observed peak maxima estimated from ref 8. Asterisks show peaks common to cobalt and nickel spectra.

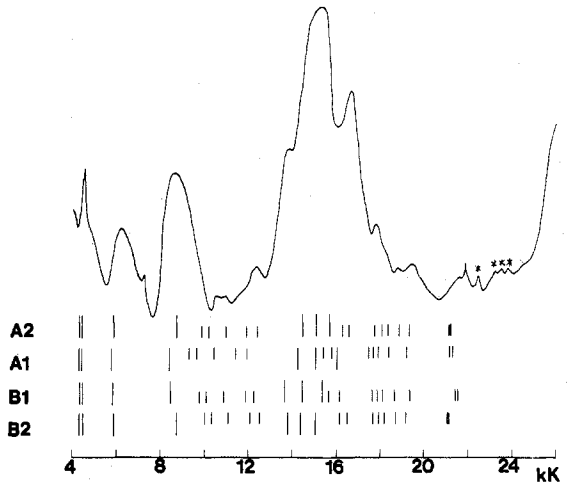

Figure 3. Tetra-*n*-butylammonium tribromo(quinoline)nickelate unpolarized crystal transmission spectrum at ca. 4 K. Bars indicate calculated eigenvalues for assignments A and B (see text): triplets and singlets are marked by long and short bars, respectively. Asterisks show peaks common to cobalt and nickel spectra.

quinoline, respectively, and e_π(Br), $e_{\pi\perp}$(Q), and $e_{\pi\parallel}$(Q), representing π interactions, where $\perp$ and $\parallel$ refer to the quinoline plane.

$Co(Q)Br_3^-$. Several preliminary calculations made clear that the effects of parameter correlations are such that a unique determination of all, or even most, variables is not possible by fitting to the susceptibilities alone. The magnetism did prove important, however, in refining fits established from the optical and ESR spectra. Those parts of the spectrum in Figure 2, which are obviously to be assigned as spin-allowed transitions, occur as three bands at ca. 4800, ca. 7200, and ca. 15 000 cm^{-1}. The more resolved, and polarized, spectra of Bertini et al.[8] suggest that the band at 7200 cm^{-1} comprises two energetically close transitions and that the broader feature centered at 15 000 cm^{-1} involves three transitions: the latter are assigned by them as components of the ^4P term. Overall approximate agreement with these spectral features, together with the crystal magnetism, is found with the following parameter set: $e_\sigma(Br) \approx e_\sigma(Q) \approx 3000$–$4000$ cm^{-1}, $B \approx 600$–700 cm^{-1}, $e_\pi(Br) \approx 900$ cm^{-1}, $e_{\pi\perp}(Q) \approx -500$ cm^{-1}, $e_{\pi\parallel}(Q) \approx 0$, $\zeta \approx 400$ cm^{-1},

$k \approx 0.9$. Without recourse to the ESR g values, we were unable to sharpen these estimates further, although we note that lower values of e_π(Br) lead to a spin-quartet band lying close to the transparent region in the spectrum just above 5500 cm^{-1}. The requirements for simultaneously reproducing the ESR spectrum,[9] however, proved much more exacting.

We note at once that an initial calculation of the molecular **g** tensor with the parameter set above yielded fair qualitative agreement with the experiment: this was characterized by two low g values on either side of 2.00 and one large value in the region 5–6. Further, the orientations of these principal g values, and of those discussed in the following paragraphs, were in satisfactory agreement with the experiment. The detailed and quantitative reproduction of both optical and ESR spectra was only achieved, however, after exhaustive calculations in which all interelectron repulsion, AOM, and spin–orbit coupling parameters were varied. Principal g values within 0.03 of the observed values[9] were obtained, by using the complete spin-quartet basis, for the following parameter set: $B = 670$ cm^{-1}, $e_\sigma(Br) \approx e_\sigma(Q) = 3500 \pm 300$ cm^{-1}, $e_\pi(Br) = 900$ cm^{-1}, $e_{\pi\perp}(Q) = -600 \pm 100$ cm^{-1}, $e_{\pi\parallel}(Q) = 0 \pm 200$ cm^{-1}, $\zeta = 400$ cm^{-1}, $k = 0.95$. Reproduction of the magnetic susceptibility was simultaneously satisfactory, and the calculated spin-allowed spectrum placed one transition just below 4900 cm^{-1}, two under the peak at 7200 cm^{-1}, and three within the envelope at 15 000 cm^{-1}. At this stage in the analysis, we enlarged the basis to include all 120 components of the complete d^7 configuration.

With the same parameter set as above, but taking F_2 and F_4 values leading to calculated spin doublets around 10 000 cm^{-1}, we found that g values were significantly and adversely affected by the inclusion of the spin-doublet manifold.[15] The overall effect was to decrease the calculated anisotropy, shifting all principal g values by up to 0.2: the susceptibilities were also changed, but agreement with the experiment was not markedly worsened. One characteristic of the spin-doublet spectrum so calculated was the placing of a group of doublets spanning an energy range 1500–2000 cm^{-1} within the gap between the spin quartets at 7200 and 15 000 cm^{-1}. Accordingly we assign the broad, weak spectral feature centered at ca. 12 200 cm^{-1} (Figure 2) to multiple spin-doublet components. Our final refinement of parameters has been based therefore on the simultaneous reproduction of the spin-allowed spectrum, these weak doublets at 12 000 cm^{-1}, and indeed the doublet spectrum above 16 000 cm^{-1}, the **g** tensor and the χ tensor. Reproduction of the **g** tensor was the most exacting requirement so far as e_π(Br) is concerned; the doublet spectrum established F_2 and F_4 values, which were only varied such that B was held fixed to satisfy the quartet spectrum; the need to avoid placing a spin quartet at 5500 cm^{-1} also contributed to the determination of e_π parameters for both bromine and quinoline ligands; reproduction of both **g** and χ tensors established optimal ζ and k values. Final parameter values for the cobalt complex, so determined, are as follows: $F_2 = 1060 \pm 10$ cm^{-1}, $F_4 = 78 \pm 2$ cm^{-1}, $e_\sigma(Br) = 3000 \pm 300$ cm^{-1}, $e_\sigma(Q) = 3500 \pm 300$ cm^{-1}, $e_\pi(Br) = 450 \pm 50$ cm^{-1}, $e_{\pi\perp}(Q) = -500 \pm 200$ cm^{-1}, $e_{\pi\parallel}(Q) = 0 \pm 100$ cm^{-1}, $\zeta = 450 \pm 35$ cm^{-1}, $k = 1.00$–0.95. The sensitivity of fit may be illustrated by noting that a change of 5 cm^{-1} in F_4 (together with a concomitant change in F_2 to hold B fixed) shifts the doublet spectrum by ca. 600 cm^{-1}, roughly monotonically throughout the whole spectral range. At the same time, calculated g values shift by up to 0.1, a change which may be compensated by an alteration in e_π(Br) of ca. 25 cm^{-1}.

(15) The importance of including doublets into the calculation of magnetic properties of d^7 complexes has also been noted by D. J. Mackey, S. V. Evans, and R. F. McMeeking, *J. Chem. Soc., Dalton Trans.*, 160 (1978).

Table VII. Tetra-*n*-butylammonium Tribromo(quinoline)nickelate: Comparison of Observed and Calculated Term Energies (cm^{-1}) for Assignments A and B (See Text)[a]

calcd			calcd	
A2	A1	obsd spectral peak	B1	B2
39 044	*38 429*		*39 274*	*39 399*
21 321	*21 735*	21 850	*21 930*	*21 238*
21 247	*21 644*	21 625	*21 848*	*21 173*
19 418	*19 606*	19 425	*19 729*	*19 258*
18 935	*18 808*	18 750	*18 959*	*18 790*
18 439	*18 318*	18 250 sh	*18 455*	*18 279*
18 166	*18 127*		*18 242*	*18 011*
17 844	*17 853*	17 775	*18 016*	*17 730*
16 677	16 454	16 610	*16 456*	*16 565*
16 356	*16 184*		*16 029*	*16 230*
15 816	*15 849*	15 150	15 715	15 105
15 179	15 462		14 755	14 460
14 573	14 637			
vibration ?		13 790	13 989	13 881
12 486	*12 319*	12 350	*12 645*	*12 546*
12 003	*11 821*	11 700 sh	*12 192*	*12 110*
11 048	*10 796*	11 050	*11 185*	*11 160*
10 282	*10 027*	10 550	*10 380*	*10 366*
9 956	*9 714*	8 550	*10 094*	*10 068*
8 802	8 817		8 765	8 779
5 966	6 149	6 150	6 161	5 976
4 539	4 781	4 760	4 792	4 549
4 404	4 702		4 714	4 414
2 620	2 752		2 730	2 606
1 046	1 092		1 098	1 052
0	0		0	0

[a] Calculated triplet term energies are averaged over spin multiplets; triplets are in roman type and singlets in italics.

Table VIII. Tetra-*n*-butylammonium Tribromo(quinoline)cobaltate: Comparison of Observed and Calculated Term Energies (cm^{-1}) for Parameter Values Listed in Table X[a]

calcd	obsd	calcd	obsd[b]
44 332		*18 091*	17 900
43 893		*17 746*	17 700
43 602		*17 476*	17 540
43 309		*17 267*	
42 706		*16 920*	
29 872		*16 699*	16 600
29 588		*15 472*	15 900
29 480		15 261	15 600
28 751		*15 042*	15 300
28 463		14 630	14 900
28 227		*14 472*	14 700
28 081		*14 416*	14 600
24 008	23 950	14 365	
23 688	23 650 ?	*13 228*	13 200 sh
22 227	22 350	*12 527*	
21 766	21 800	*12 335*	12 250
21 609		*12 113*	
21 184	21 200	*11 611*	
20 887		7 733	7 200
20 577		6 945	6 800
20 229	19 900	4 949	4 500
19 827		4 155	
19 567	19 400	3 805	
18 673	18 600	2 755	
18 442	18 400	0	

[a] Quartet term energies (roman type) and doublets (italics) are averaged over spin multiplets. [b] Observed quartet energies taken from ref 8; doublets estimated from this work and Figure 2.

The calculated and observed **g** tensors are compared in Table VI. Comparisons between observed and calculated spectral transitions are given in Table VIII and Figure 2. We have been able to account for all observed spectral features in the "doublet regions" between 16 000 and 24 000 cm^{-1}, though without assignment. Four peaks, marked with asterisks

in Figures 2 and 3, are not assigned as d–d transitions, occurring in both cobalt and nickel complexes. The bracketed observed transition energies between 14 600 and 15 900 cm^{-1} in Table VIII have been estimated, with some difficulty, from the spectral drawings in ref 8. Our calculations show that the degree of doublet–quartet mixing in this region varies between 10 and 40%, the spin designations quoted in Table VIII representing only the dominant species in each case.

$Ni(Q)Br_3^-$. As for the cobalt complex, several preliminary calculations made clear that acceptable, if not optimal, reproduction of the paramagnetism is possible for a wide range of, though by no means all, parameter values. The tactic followed, therefore, has been to seek parameter values which reproduce the spectrum, using the paramagnetism to sharpen such estimates further.

The relative intensities of the spectral bands in Figure 3 suggest that we assign peaks at 4000–5000, 6200, 8500, and 13 500–17 000 cm^{-1} as spin-allowed transitions, the latter range spanning components of ^3P and the remainder of ^3F. Eigenvalues were initially calculated for parameter values in the following ranges: $e_\sigma(Br) = e_\sigma(Q) = 2500–7000$ cm^{-1}, $e_\pi(Br) = 0–2000$ cm^{-1}, $e_{\pi\perp}(Q) = -1000–+1000$ cm^{-1}, $e_{\pi\parallel}(Q) = -500–+500$ cm^{-1}, $\zeta = 200–515$ cm^{-1}, $B = 300–1000$ cm^{-1}. The calculations confirm that the energy region 13 500–17 000 cm^{-1} *is* spanned by spin-triplet components of ^3P and none from ^3F, as expected. Further refinements are all based upon calculations spanning the complete 45-fold d^8 configuration. The central issue to emerge throughout the reproduction of the observed spectrum of this complex stems from the observation that no combination of interelectron repulsion or angular overlap parameters yields spin-triplet eigenvalues which reproduce all three peaks in the 13 800–16 600-cm^{-1} region. The overall splitting of the ^3P term is never calculated greater than 1800 cm^{-1}, instead of 2800 cm^{-1} apparently observed. Parameter values which reproduce the spectral region below 10 000 cm^{-1} simultaneously predict a ^3P splitting of about 1500 cm^{-1}. Satisfactory fits are obtainable with e_σ values in the range 3500–4500 cm^{-1} when taken with appropriately correlated $e_\pi(Br)$ values. Within these ranges, a spin-forbidden transition is never calculated to lie near 13 800 cm^{-1} while simultaneous reproduction of most other spin-forbidden features is achieved. Accordingly, we have considered two sets of assignments of the 13 800–16 600-cm^{-1} region of the spectrum.

Assignment A. Here we place two components of the ^3P term within the broadest peak centered at ca. 15 300 cm^{-1} and one corresponding to the sharper feature at 16 600 cm^{-1}. The peak at ca. 13 800 cm^{-1}, which appears only as a shoulder at 80 K, is assigned as a vibrational component of, perhaps the lowest energy part of, the spin-allowed transitions near 15 300 cm^{-1}. Depending upon the exact placing of the lowest ^3P component, this proposed vibrational splitting could be as small as ca. 750 cm^{-1}. Quantitative fitting of the spectrum proceeded first by reproducing the spin-allowed transitions and then, holding the established Racah B value constant, the spin-forbidden peaks by variation of F_2 and F_4. As mentioned above, satisfactory fits were obtained for a fairly wide range of e_σ values. The detailed reproduction of most spectral (and all magnetic) data is essentially identical throughout this range of coupled e_σ and $e_\pi(Br)$ parameter values. The only distinguishing feature in the range is the calculated ^3P splitting, being ca. 1200 cm^{-1} for $e_\sigma \approx 3500$ cm^{-1} and ca. 1800 cm^{-1} for $e_\sigma \approx 4500$ cm^{-1}. The larger splitting is to be favored in terms of the distribution of transition energies under the broad peak at ca. 15 300 cm^{-1} and of the proximity of spin-triplet and -singlet transition in the region which may augment intensity stealing processes. On the other hand, the lower values of e_σ correspond more closely with those values determined for the cobalt complex. In Figure 3 and Table VII, we detail fits, labeled A1 and A2, corresponding to the following optimized parameter sets: (A1) $e_\sigma(Br) = 4500$ cm^{-1}, $e_\sigma(Q) = 4000$ cm^{-1}, $e_\pi(Br) = 1100$ cm^{-1}, $e_{\pi\perp}(Q) = -500$ cm^{-1}, $e_{\pi\parallel}(Q) = 0$, $B = 720$ cm^{-1}, $F_2 = 1070$ cm^{-1}, $F_4 = 70$ cm^{-1}, $\zeta = 250$ cm^{-1}, $k = 0.73$; (A2) $e_\sigma(Br) = 3600$ cm^{-1}, $e_\sigma(Q) = 3600$ cm^{-1}, $e_\pi(Br) = 500$ cm^{-1}, $e_{\pi\perp}(Q) = -600$ cm^{-1}, $e_{\pi\parallel}(Q) = 0$, $B = 720$ cm^{-1}, $F_2 = 1090$ cm^{-1}, $F_4 = 74$ cm^{-1}, $\zeta = 250$ cm^{-1}, $k = 0.73$.

Assignment B. In this case we assign one component of ^3P to lie at ca. 13 800 cm^{-1} and again two within the broader feature centered at 15 300 cm^{-1}. The sharper peak at 16 600 cm^{-1} is now assigned as spin forbidden with an intensity augmented by "stealing" from the nearby spin triplets. Following the same procedures as above, we have optimized two parameter sets to reproduce the paramagnetism and all spectral features. Again the larger e_σ values yield a larger ^3P splitting and might be favored but for the lower e_σ values determined for the cobalt complex. Details shown in Figure 3 and Table VII correspond to the following parameter sets: (B1) as for A1, but $B = 670$ cm^{-1}, $F_2 = 1070$ cm^{-1}, and $F_4 = 80$ cm^{-1}; (B2) as for A2, but $B = 670$ cm^{-1}, $F_2 = 1070$ cm^{-1}, and $F_4 = 80$ cm^{-1}. Again the four small features in the energy range 22 000–24 000 cm^{-1} (marked with asterisks in Figures 2 and 3) occur in the spectra of both nickel and cobalt complexes, so that their nonreproduction by the present calculations appears to confirm that their origin does not lie in the ligand field d–d spectrum.

The differences between assignments A and B are small. Our prejudice is for B, but a clear rejection of A is not possible from the present study. Calculated magnetic properties differ insignificantly between the four parameter sets above and are in essentially perfect agreement with experiment, as discussed below. While it is disappointing not to have defined the e_σ values, together with the correlated $e_\pi(Br)$ value more precisely in the nickel complex, we note that all optimized parameter sets show quinoline to act as a significant π acceptor with $e_{\pi\perp}(Q) = -500 \pm 200$ cm^{-1}. Further, calculations show that $e_{\pi\parallel}(Q) = 0 \pm 100$ cm^{-1}, as expected.

Comparison between Observed and Calculated Susceptibilities. For both nickel and cobalt complexes the final agreement between observed and calculated susceptibility tensors is excellent throughout the complete 20–300 K temperature range. The agreement is shown in two ways. In Figure 1 were shown projections of the observed susceptibility ellipsoids down principal axes. Similar projections of the calculated ellipsoids which are at the same temperature and which are drawn on the same scale superimpose these within the thickness of drawn curves: agreement is even closer at higher temperatures. The numerical correspondence between calculated and experimental susceptibilities is shown in Table IX in which data are given for each of the six independent tensor elements (relative to the orthogonalized crystal frame) at each of six representative temperatures.

Zero-Field Splittings and Ground-State Wavefunctions. The formal $^3T_1$ (T_d parentage) of the nickel complex splits in the low-symmetry field, spanning an energy range of some 2800 cm^{-1}. The lowest orbital component itself gives rise to three distinct components, under the combined effect of the ligand field and spin–orbit coupling, with energies 0, 11, and 42 cm^{-1} relative to the ground state: these values correspond to the parameter set B1 (and in Table X).

The ground orbital singlet of the cobalt complex splits into two Kramer doublets whose energy separation calculated with the parameter set above (and in Table X) is 23 cm^{-1}. Bencini and Gatteschi[9] argued that this zero-field splitting should be at least 5 cm^{-1} and also that the ground state corresponds to the $M_s = \pm^1/_2$ doublet rather than to $M_s = \pm^3/_2$. A description in these terms depends upon the quantization axis,

Table IX. Comparisons between Observed and Calculated Susceptibility Tensors Using Parameters Listed in Table X[a]

		T, K					
		295	155	95	75	45	25
		(a) Nickel Complex					
χ_{11}	calcd	37	65	99	119	168	211
	obsd	43	71	104	123	163	188
χ_{22}	calcd	62	116	192	248	430	802
	obsd	59	120	198	257	438	779
χ_{33}	calcd	47	85	134	167	265	426
	obsd	49	92	145	183	283	446
χ_{21}	calcd	3	7	12	17	34	77
	obsd	0	2	3	5	9	17
χ_{31}	calcd	0	0	0	0	0	0
	obsd	2	3	4	5	8	15
χ_{32}	calcd	−9	−18	−33	−46	−95	−216
	obsd	−6	−18	−34	−48	−98	−235
		(b) Cobalt Complex					
χ_{11}	calcd	101	205	361	584	981	1456
	obsd	92	192	338	545	906	1329
χ_{22}	calcd	86	159	254	364	506	617
	obsd	88	161	263	383	545	685
χ_{33}	calcd	89	174	289	435	652	861
	obsd	84	165	275	412	608	796
χ_{21}	calcd	−4	−10	−23	−45	−94	−164
	obsd	5	−4	−8	−15	−30	−43
χ_{31}	calcd	0	0	0	0	−3	−8
	obsd	−1	0	1	−3	−11	−26
χ_{32}	calcd	3	8	18	36	75	125
	obsd	1	9	22	45	94	155

[a] Susceptibilities in cgsu × 10^4 relative to orthogonalized crystal frame used in Table III.

Table X. Parameter Values Giving Best Reproduction of Susceptibility Tensors and Optical and ESR Spectra (As Appropriate)[a]

parameter	Ni complex[b]	Co complex
F_2	1070 (10)	1060 (10)
F_4	80 (2)	78 (2)
B	670 (10)	670 (10)
e_σ(Br)	4500 (300)	3000 (300)
e_σ(Q)	4000 (300)	3500 (300)
e_π(Br)	1100 (200)	450 (50)
$e_{\pi\perp}$(Q)	−500 (100)	−500 (200)
$e_{\pi\parallel}$(Q)	0 (100)	0 (100)
ζ	250 (25)	450 (35)
k	0.73 (0.05)	1.00 (0.05)

[a] All energies are in cm^{-1}. [b] Estimated errors corresponding to optimization of parameter set B1.

of course, but we *do* find for a z axis taken parallel to the (very approximate) triad, Co–N, that the ground state *is* predominantly as described by Bencini and Gatteschi. Accordingly no special relaxation of the usual selection rules need be invoked to explain the ESR signals.

Conclusions

We have analyzed the optical spectrum and susceptibility tensor of tetra-*n*-butylammonium tribromo(quinoline)nickelate and the optical and ESR spectra and paramagnetism of the analogous cobaltate complexes within a generalized, symmetry-unrestricted ligand field model. Excellent reproduction of all properties has been achieved for the parameter sets given in Table X.

The net acceptor properties of the nickel ion are probably greater than for the cobalt ion in line with established trends in effective nuclear charge and the spectrochemical series. In both complexes, the quinoline ligands act as moderate π acceptors. The value $e_{\pi\perp}(Q) = -500$ cm^{-1} may be compared with those of +50 cm^{-1} in trans octahedral $M(py)_4NCS_2$, where M = Co(II) or Fe(II),[2] of +900 cm^{-1} for the imine nitrogen donor atoms in a tetrahedral[10] and a five-coordinate[16] nickel(II) complex, of −1000 to −2000 cm^{-1} for the phosphine groups in some tetrahedral nickel(II) and cobalt(II) complexes,[17] or of +1000 cm^{-1} for the imine and 0 ± 200 cm^{-1} for the pyridine nitrogen donors in some seven-coordinate species.[18,19] There is no evidence for metal–ligand π bonding *in* the quinoline plane in either complex, as is expected.

The value found for the spin–orbit coupling coefficient ζ appears normal for the cobalt complex but anomalously low for the nickel complex. We emphasize that the value given in Table X was carefully established after many variations of all other parameters, but no figure outside the quoted errors leads to satisfactory reproduction of the experimental susceptibilities. A somewhat low value for ζ was also found[17] in the tetrahedral complexes $Ni(PPh_3)_2X_2$ (X = Cl, Br), and there is some similar evidence from an earlier study[20] of $(Et_4N)_2NiCl_4$. The low ζ value found here is not associated either with excessively reduced interelectron repulsion parameters or with very low k values; nor does the electronic d manifold describe a situation close to orbital degeneracy, so we do not believe the low ζ value is associated with the Ham effect.

Acknowledgment. We are grateful to Drs. J. E. Davies and R. F. McMeeking for discussions and the use of their computer programs. We also thank the Royal Society, London, for the award of a Rutherford Scholarship and the New Zealand University Grants Committee for financial support (both to L.R.H.).

Registry No. $[(n\text{-}C_4H_9)_4N][Co(C_9H_7N)Br_3]$, 52524-44-4; $[(n\text{-}C_4H_9)_4N][Ni(C_9H_7N)Br_3]$, 22388-71-2.

(16) D. A. Cruse and M. Gerloch, *J. Chem. Soc., Dalton Trans.*, 1613 (1977).
(17) J. E. Davies, M. Gerloch, and D. J. Phillips, *J. Chem. Soc., Dalton Trans.*, 1836 (1979).
(18) M. Gerloch, I. Morgenstern-Baderau, and J. P. Audière, *Inorg. Chem.*, in press.
(19) M. Gerloch and I. Morgenstern-Baderau, *Inorg. Chem.*, in press.
(20) M. Gerloch and R. C. Slade, *J. Chem. Soc. A*, 1022 (1969).